Physica D 238 (2009) 506–515

Contents lists available at ScienceDirect

Physica D

journal homepage: www.elsevier.com/locate/physd

Pacemaker-guided noise-induced spatial periodicity in excitable media

Marko Gosak, Marko Marhl, Matjaž Perc *

Department of Physics, Faculty of Natural Sciences and Mathematics, University of Maribor, Koroška cesta 160, SI-2000 Maribor, Slovenia

ARTICLE INFO

Article history:
Received 29 August 2007
Received in revised form
12 November 2008
Accepted 22 November 2008
Available online 3 December 2008
Communicated by A. Pikovsky

PACS:
05.45.-a
05.40.-a
89.75.Kd

Keywords:
Pacemaker
Excitable media
Noise
Pattern formation

ABSTRACT

We study the impact of subthreshold periodic pacemaker activity and internal noise on the spatial dynamics of excitable media. For this purpose, we examine two systems that both consist of diffusively coupled units. In the first case, the local dynamics of the units is driven by a simple one-dimensional model of excitability with a piece-wise linear potential. In the second case, a more realistic biological system is studied, and the local dynamics is driven by a model for calcium oscillations. Internal noise is introduced via the τ-leap stochastic integration procedure and its intensity is determined by the finite size of each constitutive system unit. We show that there exists an intermediate level of internal stochasticity for which the localized pacemaker activity maps best into coherent periodic waves, whose spatial frequency is uniquely determined by the local subthreshold forcing. Via an analytical treatment of the simple minimal model for the excitable spatially extended system, we explicitly link the pacemaker activity with the spatial dynamics and determine necessary conditions that warrant the observation of the phenomenon in excitable media. Our results could prove useful for the understanding of interplay between local and global agonists affecting the functioning of tissue and organs.

1. Introduction

It is a well-established fact that noise can have a profound effect on the dynamics of nonlinear systems [1–3]. Thereby, noise alone often suffices to induce coherent system behavior [4]. Examples range from noise-induced order in isolated systems [5–10], one-dimensional arrays [11–14] and planar media [15–21], to coherent behaviors in small-world networks [22–25]. Excitability arguably represents the most viable system state warranting the observation of fascinating noise-induced phenomena [3,26]. Remarkably, noise can also enhance [27] or even induce [28] excitable behavior in systems where otherwise oscillations and frigidness to weak external perturbations would reign. A conceptually similar transition to excitability, as reported in [28], was recently related to a form of noise-memory [29] and also the variability of constitutive system units [30]. Remarkably, the potentially constructive role of noise has also been studied in the context of signal propagation. The phenomenon has been reported in arrays of bistable oscillators [31–33], in monostable media [34] and in sub-excitable media [35,36]. Noise sustained propagation has also been considered in a one-way coupled chain of excitable oscillators [37] and in a variety of dynamical systems that exhibit a coexistence of a spatial periodic state and a homogeneous state [38]. In [39] travelling waves in an array of sub-excitable units under different types of noise and periodic forcing have been studied. Interestingly, Ullner et al. [40] have reported a conceptual similar phenomenon, called vibrational propagation. They have revealed that a low frequency signal can be efficiently propagated through an array of coupled excitable elements in case of an additional high frequency forcing that is applied to the whole array. Despite the vast amount of literature dedicated to the study of effects of noise on nonlinear systems, the subject remains vibrant, offering intriguing scientific challenges.

A particularly lively subject appears to be the study of the impact pacemaker activity can have on excitable systems. Recently, Chigwada et al. [41] have introduced so-called resonance pacemakers, able to induce successive travelling waves in a quiescent excitable chemical medium via local modulations of excitability, whereby wave-emitting pacemakers in the context of the Belousov–Zhabotinsky medium have already been studied before [42,43]. Several studies have also been performed in order to investigate the impact of pacemaker activity on the functioning of cardiac tissue [44]. The physical and physiological mechanisms of excitation spreading through calcium-activated channels in the cleft between adjacent cardiac myocytes are well understood due to the Luo–Rudy model [45–47], incorporating all ionic currents through the different membrane channels in the different compartments of the myocytes. From a more mathematical perspective, synchronization of oscillators [48], and formation of self-organized pacemakers [49] have also been

* Corresponding author.
E-mail address: matjaz.perc@uni-mb.si (M. Perc).

0167-2789/$ – see front matter © 2008 Elsevier B.V. All rights reserved.
doi:10.1016/j.physd.2008.11.007

reported. In [50] a systematic study of firing waves in oscillatory media has been performed. Moreover, Nagai et al. [51] have studied pacemaker activities in the case of chick embryonic heart cells cultured in an annular geometry. On the basis of fluorescence from calcium sensitive dyes, propagation of pacemaker-triggered intracellular calcium waves has been observed. Jacquemet [52] studied the impact of fibroblasts (non-excitable cells) that are sometimes coupled with excitable cells, whereas Gutman et al. [53] focused on a heterogeneous reaction–diffusion medium consisting of two adjoining uniform regions. The latter system set-up allows an abnormal domination of the low natural frequency of the oscillatory regime over the whole medium. This abnormal frequency-locking phenomenon could explain some dynamical properties of the cardiac pacemaker. Related to the subject of the present paper is also the study by Stich and Mikhailov [54], who investigated pacemaker-induced target patterns in a heterogeneous two-dimensional reaction–diffusion system governed by the complex Ginzburg–Landau equation, albeit in the absence of noise.

Noteworthy pacemaker activities have also been investigated in media with different topologies. Kori and Mikhailov [55] have studied several classes of random networks consisting of identical phase oscillators that were entrained by a pacemaker. In particular, the entrainment frequency window of the network in dependence on the network depth was examined. Radicchi and Meyer-Ortmanns [56] have studied Kuramoto oscillators on n-dimensional regular topologies with nearest neighbor interactions, specifically examining the connections between critical pacemaker frequency and system size or depth of the network. Moreover, in [57] the role of weak pacemaker activity and noise on excitable small-world networks have been investigated, whereby it has been shown that, for intermediate coupling strengths, randomness in the coupling can enhance the response of the array in a resonant manner.

Intrinsic fluctuations are an unavoidable feature of all chemically reacting systems and are especially apparent in systems with relatively small number of molecules. Particularly in cellular processes, where the number of molecules defining the process is often low, the stochastic effects must be taken into account in order to firmly describe such systems. Conventionally, the stochastic dynamics of those systems is accurately described by the master equation, which however is very difficult to solve, especially when dealing with systems that exhibit quite complex dynamics. In view of that, Gillespie [58] derived a numerical procedure that simulates the time evolution of a given stochastic system. The algorithm makes exact numerical calculations within the framework of stochastic formulation, without having to deal with the master equation. Therefore, as it has been nicely presented by Gracheva et al. [59], this method is very convenient for stochastic simulations of complex cellular processes that are originally described by deterministic rate equations. In this manner, randomness that is inherent in chemical reactions is taken into account, as well as the fact that, due to the final system size, the concentration of molecular species can only vary by a discrete amount.

In the present study, we extend the scope of pacemaker activity in excitable media, specifically by studying the impact of subthreshold pacemaker activity in the presence of internal stochasticity. For this purpose, we study two systems exhibiting these features. In the first place, we employ a simple one-dimensional excitable system with a piece-wise linear potential as the constitutive unit of the two-dimensional medium. Importantly, the studied system incorporates only the essential dynamical features that are required for the generation of excitable behavior. As such, it addresses excitability as a canonical property of several physiologically accurate models [3]. An advantage thereof is that the dynamics of the medium is analytically tractable and allows the identification of general conditions warranting the observation of presently reported results. With the aim to apply our ideas on a biologically more realistic system, we further study the impact of a subthreshold pacemaker and internal fluctuations on the spatial dynamics of diffusively coupled cells. We employ a mathematical model for calcium oscillations that drives the local excitable dynamics of individual cells and show that a very similar behavior is found as for the minimal model.

The regarded media is subjected to localized subthreshold perturbations in form of a simple periodic pulse trains. We show that, in dependence on the level of internal stochasticity, the subthreshold pacemaker is able to induce ordered spatial waves in a resonant manner. Importantly, in the zero-noise limit, the pacemaker is unable to evoke excitations in the medium. Thus, the internal stochasticity is an essential ingredient warranting the emergence and propagation of periodic spatial waves. Besides presenting conclusive evidence for pacemaker-guided noise-induced spatial periodicity in the studied media, we also determine necessary conditions that warrant the observation of the phenomenon and explicitly link the pacemaker activity with the spatial dynamics. Via an analytical treatment of the minimal model, we find that in order to guide the spatial dynamics of noisy excitable media, subthreshold pacemakers must be introduced to spatially extended systems whose constitutive units incorporate a finite refractory time, preventing unwanted spreading of excitatory events. Remarkably, the refractory time is a typical inherent feature of many biological systems. Thus we show that, for a biologically more realistic model, describing cellular calcium signalling, the finite refractory time characterizing local cellular dynamics is of crucial importance for a successful regulation of pacemaker-driven spatial dynamics of diffusively coupled cells. The obtained results could prove useful for shedding light on the interplay between global (being the stochasticity) and local (being the pacemaker) agonists that affect the functioning of tissue or even whole organs, as discussed at the end.

The paper is structured as follows. Section 2 is devoted to the description of the simple model for excitable media and pacemaker activity as well as the introduction of internal noise. In Sections 3 and 4 evidence for the pacemaker-guided spatial periodicity and the analytical estimations is presented, respectively. In Section 5 we perform a similar examination as in Section 3, but for the biologically more realistic system, where the impact of internal stochasticity and a subthreshold pacemaker on the spatial dynamics of Ca^{2+} waves is studied. In the last section we summarize the results and outline possible biological implications of our findings.

2. Mathematical model

As already specified in the Introduction, we presently use a simple one-dimensional excitable system with a piece-wise linear potential as the constitutive unit of the studied medium. The employed dynamical system was proposed by Pradines et al. [26] to study the essential role of slow and fast dynamics for the observation of coherence resonance [8]. It takes the form

$$\frac{\mathrm{d}u}{\mathrm{d}t} = f(u) = (1-a)\Theta(u_c - u) + b\,\Theta(u - u_c), \tag{1}$$

where $0 \leq u < 2\pi$ is the phase of the system, Θ is the Heaviside function, $u_c > 0$ is the firing threshold, whilst parameters $a > 1$ and $b > 0$ determine the slow and fast kinetics of the system for $u < u_c$ and $u > u_c$, respectively. The model, described by Eq. (1) is a one-dimensional phase model of excitability, where the dynamics is described by an amplitude and a phase, where the letter variable incorporates systems excitability. The term describing the velocity of the phase $f(u)$ is 2π periodic, since the phase is a cyclic function.

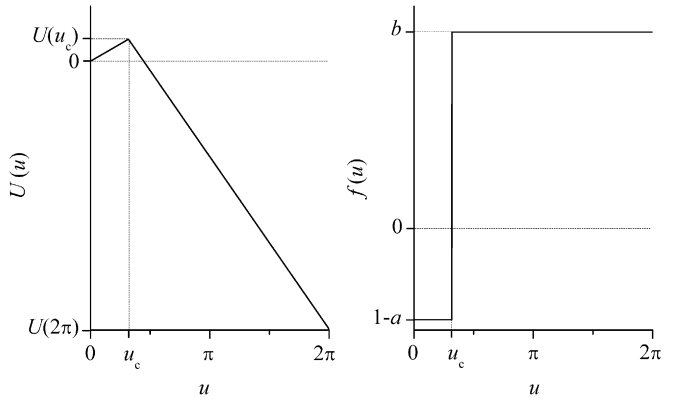

Fig. 1. The potential $U(u)$ (left) and the corresponding function $f(u)$ (right), which determines the velocity of the changes of u, as defined by Eq. (1).

Consequently, the corresponding potential, which is defined as $U(u) = -\int f(u)\mathrm{d}u$, is also 2π periodic. In order to represent and elucidate the system's excitable behavior we show in Fig. 1 the form of the potential and the subsequent velocity of the phase $f(u)$, defined by Eq. (1). We can observe that at $u = 0$ the potential possesses a minimum, which represents the system's excitable steady state (by considering that $a > 1$ and $b > 0$). The maximum of the potential at $u = u_c$ represents the threshold. In case of minor deviations from the excitable steady state ($u < u_c$) the system remains in the rest state, which represents the system's slow dynamics [$f(u) = 1 - a$]. However, when perturbations of the excitable steady state provoke the phase variable to exceed u_c, the system sets into the firing state, which represents the system's fast dynamics [$f(u) = b$] and is characterized by large-amplitude spikes ($u = 2\pi$). It should be emphasized that the model, introduced by Pradines et al. is a piecewise linear version of the Adler model [60], where the effective potential is a tiled cosine function. This model is also related to the Θ neuron model developed in the neuroscience [61].

Importantly, by setting $b \gg (a - 1)$ the model given by Eq. (1) quickly re-occupies the steady state after each excitation and is thus virtually instantly ready to get excited again by the same weak perturbation that evoked the preceding excitation. Hence, $u = 0$ acts as an excitable steady node. We note that, on the contrary, excitable foci are often characterized by long refractory times during which they are extremely robust to external influences. Importantly, however, long refractory times characterize several biological processes, one of the most prominent examples being oscillations of free cytosolic calcium concentration [62,63] as presented in Section 5. Thus, the mathematical concept of a stable node is often at odds with real-life situations, where an excitation cannot occur immediately after the former excitation. To account specifically for this fact, we introduce an additional refractory time t_r to Eq. (1) that sets in after each excitation $u = 2\pi$. During t_r we set $u \equiv 0$ independent of the external forcing. In Section 4, we will show that finite refractory times are in fact essential for the observation of pacemaker-guided spatial periodicity in excitable media, as will be reported in Section 3.

The above one-dimensional model is used as the constitutive unit for the spatially extended system that takes the form

$$\frac{\partial u_{i,j}}{\partial t} = f(u_{i,j}) + D\nabla^2 u_{i,j} + \pi_\Theta(t), \tag{2}$$

where $u_{i,j}$ is considered as a dimensionless two-dimensional scalar field on a discrete $n \times n$ square lattice with mesh size $\Delta x = 1$. The Laplacian $D\nabla^2 u_{i,j}$ is incorporated into the numerical scheme via a five-point finite-difference formula [64] $D\nabla^2 u_{i,j} = D(u_{i+1,j} + u_{i-1,j} + u_{i,j+1} + u_{i,j-1} - 4u_{i,j})$, using absorbing boundary conditions. The pacemaker $\pi_\Theta(t)$ is modelled by a periodic pulse train

$$\pi_\Theta(t) = \begin{cases} g, & (t \bmod t_\pi) \geq (t_\pi - w) \\ 0, & \text{else,} \end{cases} \tag{3}$$

where t_π is the oscillation period of the pacemaker, w is the width and g the amplitude of each pulse, respectively. Moreover, the subscript Θ denotes a subset of the $n \times n$ square lattice, representing those spatial units to which the pacemaker is introduced. Presently, $\Theta \in [n/2 - 1, n/2 + 1]$ in both dimensions of the spatial grid, thus introducing the pacemaker activity to the central 9 units of the medium. The spatially extended system given by Eq. (2) is simulated with the Gillespie's τ- leap method [65] (being an approximation of the exact stochastic simulation algorithm [58]), which introduces internal stochasticity into the reaction–diffusion scheme.

Importantly, since we are studying the dynamics of a partial differential equation rather than a chemical reaction scheme, the τ-leap method is implemented similarly to that exemplified by Gracheva et al. [59] or Li et al. [10], where reaction rates are ascribed to fluxes constituting the differential equation. These reaction rates determine, through a Poissonian distribution, how much the value of $u_{i,j}$ will increase or decrease in a given time interval τ. Importantly, the above is a crucial step in accommodating Gillespie's original τ-leap algorithm, initially intended for chemical reaction schemes, so that it can be formulated on the basis of a differential equation. In accordance with the reaction rates, a discrete change of the phase u of the form κ_x/χ is performed at each iteration, where χ is the effective size (volume) of each individual excitable unit and κ_x is an integer obtained from the Poissonian

$$P(r_x, \tau) = \frac{\mathrm{e}^{-r_x\tau}(r_x\tau)^{\kappa_x}}{\kappa_x!}, \tag{4}$$

where r_x ($x = 1, 2, \ldots, 7$) are reaction rates that are specified in Table 1, along with the corresponding stochastic processes. During a time interval τ, each of the seven reaction rates is evaluated and the corresponding stochastic process executed as dictated by κ_x obtained from Eq. (4).

Note that in the above scheme χ uniquely determines the level of internal noise to which the medium is exposed, since the number of particles constituting the dynamics of each excitable unit is directly proportional to χ. Consequently, small χ correspond to large levels of stochasticity while increasing values of χ eventually introduce deterministic steady state solutions in the dynamics of each individual unit and ultimately result in a quiescent medium [note that the pacemaker activity alone is unable to evoke large amplitude ($u > u_c$) excitations].

By simulating the system with the τ-leap algorithm, randomness associated with the finite number of elements composing the system is considered. Such an approach finds the expression, especially in realistic cellular processes, which are usually described by a fairly complex set of differential equations [62,63]. However, the main properties of realistic excitable systems can be quite well qualitatively captured by Eq. (1). Thus, Eq. (1) models excitability as a canonical dynamical property [66] of physiologically accurate models without taking explicitly into account specific underlying physiological details of such processes. The reason why we construct a stochastic simulation of this minimal model, is that a smooth transition to realistic systems is achieved. Namely, as we will see in Section 5, this method can be very convenient for stochastic simulations of complex cellular processes that are originally described by deterministic rate equations. In those systems, discrete changes of concentrations of molecular species are inherent, due to the finite number of reacting molecules. Similarly, the

Table 1
Reaction rates and corresponding stochastic processes entailed in a given iteration of the employed τ-leap algorithm.

Reaction rate:	Stochastic process:
$r_1 = \chi \lvert 1-a \rvert \Theta(u_c - u_{i,j})$	$u_{i,j} \to u_{i,j} - \kappa_1/\chi$
$r_2 = \chi b \Theta(u_{i,j} - u_c)$	$u_{i,j} \to u_{i,j} + \kappa_2/\chi$
$r_3 = \chi D \lvert u_{i-1,j} - u_{i,j} \rvert$	$u_{i,j} \to u_{i,j} + \kappa_3/\chi, u_{i-1,j} \to u_{i-1,j} - \kappa_3/\chi$ if $u_{i-1,j} - u_{i,j} > 0$
	$u_{i,j} \to u_{i,j} - \kappa_3/\chi, u_{i-1,j} \to u_{i-1,j} + \kappa_3/\chi$ if $u_{i-1,j} - u_{i,j} < 0$
$r_4 = \chi D \lvert u_{i+1,j} - u_{i,j} \rvert$	$u_{i,j} \to u_{i,j} + \kappa_4/\chi, u_{i+1,j} \to u_{i+1,j} - \kappa_4/\chi$ if $u_{i+1,j} - u_{i,j} > 0$
	$u_{i,j} \to u_{i,j} - \kappa_4/\chi, u_{i+1,j} \to u_{i+1,j} + \kappa_4/\chi$ if $u_{i+1,j} - u_{i,j} < 0$
$r_5 = \chi D \lvert u_{i,j-1} - u_{i,j} \rvert$	$u_{i,j} \to u_{i,j} + \kappa_5/\chi, u_{i,j-1} \to u_{i,j-1} - \kappa_5/\chi$ if $u_{i,j-1} - u_{i,j} > 0$
	$u_{i,j} \to u_{i,j} - \kappa_5/\chi, u_{i,j-1} \to u_{i,j-1} + \kappa_5/\chi$ if $u_{i,j-1} - u_{i,j} < 0$
$r_6 = \chi D \lvert u_{i,j+1} - u_{i,j} \rvert$	$u_{i,j} \to u_{i,j} + \kappa_6/\chi, u_{i,j+1} \to u_{i,j+1} - \kappa_6/\chi$ if $u_{i,j+1} - u_{i,j} > 0$
	$u_{i,j} \to u_{i,j} - \kappa_6/\chi, u_{i,j+1} \to u_{i,j+1} + \kappa_6/\chi$ if $u_{i,j+1} - u_{i,j} < 0$
$r_7 = \chi \pi_\Theta$	$u_{i,j} \to u_{i,j} + \kappa_7/\chi$

discrete change of the phase u in the minimal model can be regarded as a consequence of fictitious molecular reactions that govern the dynamics of u. Remarkably, as argued in [65,67], if the number of reacting molecules (i.e. system size χ) is large enough, the time evolution of molecular species can be approximated by the continuous Markov process defined by the chemical Langevin equation. Most importantly, in the limit of infinitely large molecular populations ($\chi \to \infty$), terms in the Langevin equation that represent noisy contributions become negligible, and the description of the dynamics alters to deterministic rate equations.

System parameters used in subsequent calculations are: $a = 1.05$, $b = 20.0$, $u_c = \pi/40$, $D = 0.30$, $t_r = 0.25$, and $n = 64$. The subthreshold pacemaker is defined by $g = \pi/8$ and $w = 0.16$, whereas the two variable parameters are χ and t_π, determining the level of internal noise and period of the pacemaker, respectively. Moreover, the system is initiated from steady state excitable conditions $u_{i,j} = 0$ for $\forall i, j$, and simulated with $\tau = 0.001$.

3. Pacemaker-guided spatial dynamics

In what follows, we will systematically analyze effects of different χ and t_π on the spatial dynamics of the medium, providing conclusive evidence that the subthreshold pacemaker activity can induce periodic waves in the spatial domain, provided the intensity of internal noise is adequately adjusted. We start by visually inspecting characteristic spatial profiles of u_{ij} obtained for different χ and t_π. Fig. 2 features the results. It is evident that there exists an intermediate value of χ (middle column), for which the pacemaker, acting on the 9 central units of the spatial grid, induces coherent periodic waves with a well-defined spatial frequency. This general observation is independent of t_π. However, as the period of the pacemaker increases (top towards bottom), the spatial frequency of excitatory waves decreases (wavelength increases). Evidently, larger levels of internal stochasticity (left column) completely overshadow the pacemaker, whereas smaller ones (right column) lend too little support to its activity to warrant a continuous triggering of the waves. Either way, the spatial dynamics become disordered, in particular lacking a well-defined spatial frequency, as the level of internal noise departs from the optimal value.

To quantify the spatial dynamics by different χ and t_π more precisely, we calculate the spatial structure function according to the equation

$$P(k_x, k_y) = \left\langle H^2(k_x, k_y, t) \right\rangle, \tag{5}$$

where $H(k_x, k_y, t)$ is the spatial Fourier transform of the u-field at a particular time t, and $\langle \ldots \rangle$ denotes the average over t. Accordingly, the spatial behavior over a long time period is considered. Moreover, we exploit the circular symmetry of $P(\vec{k})$ by calculating the circular average of the structure function [2] according to the equation

$$p(k) = \int_{\Omega_k} P(\vec{k}) \mathrm{d}\Omega_k, \tag{6}$$

where Ω_k is a circular shell of radius $k = \left|\vec{k}\right|$. Fig. 3 shows the results for different t_π by the optimal χ. Evidently, there exist a well-defined spatial frequency of excitatory events irrespective of t_π. But, as emphasized already above, the period of the pacemaker t_π clearly guides the excitatory waves as their spatial frequency $k = k_{\max}$ humbly follows the localized stimulus despite its subthreshold nature.

To quantify the ability of each particular χ to optimally amplify the subthreshold pacemaker activity, so that the latter induces most ordered spatial waves, we calculate the quantity $\rho = p(k_{\max})/\tilde{p}$, where $\tilde{p} = [p(k_{\max} - \Delta k_a) + p(k_{\max} + \Delta k_b)]/2$ is an approximation for the level of background fluctuations. Thereby, Δk_a and Δk_b mark the first local minima occurring to the left and right side of $k_{\max}$ respectively, hence determining the width of the peak around the resonantly pronounced spatial frequency. Thus, ρ measures the normalized height of the peak at $k_{\max}$ for each particular χ. Fig. 4 shows how ρ varies with χ for different t_π. It is evident that there always exists an optimal level of internal noise for which the peak of the circularly averaged structure function at $k_{\max}$ is best resolved, thus indicating the optimal entrainment of pacemaker activity on the excitable medium. Noteworthy, even without the normalization by the level of background fluctuations $\tilde{p}$, the values of $p(k_{\max})$ still exhibit a nonmonotonic outlay in dependence on the system size, with the maximum occurring by the same value of χ as in case of ρ. Evidently, there also appears to exist an optimal t_π warranting the largest ρ in dependence on χ. Nevertheless, we will show in the next section that, in fact, only a lower bound of t_π exists towards which the maximally attainable ρ decreases (as shown for $t_\pi = 0.8$ in Fig. 4), whereas the decrease of ρ by larger t_π (as shown for $t_\pi = 1.6$ in Fig. 4) is simply linked with the finiteness of the spatial grid ($n = 64$) and the resulting numerical inaccuracy of the spatial Fourier transform.

Due to the minimalistic form of the studied spatially extended system, the pacemaker activity can be explicitly linked with the dynamics of excitatory waves, and moreover, necessary conditions for the above-reported phenomenon can be derived. The next section is devoted to the accomplishment of this task.

4. Analytical estimations

For the analytical estimations, we use a slightly simplified version of the above-studied pacemaker-driven spatially extended system [see Eq. (2)]. The model is indeed only slightly simplified in the sense that we consider one single unit acting as the pacemaker. This doesn't really change the conditions simulated numerically, because the cluster of nine cells acting as pacemakers

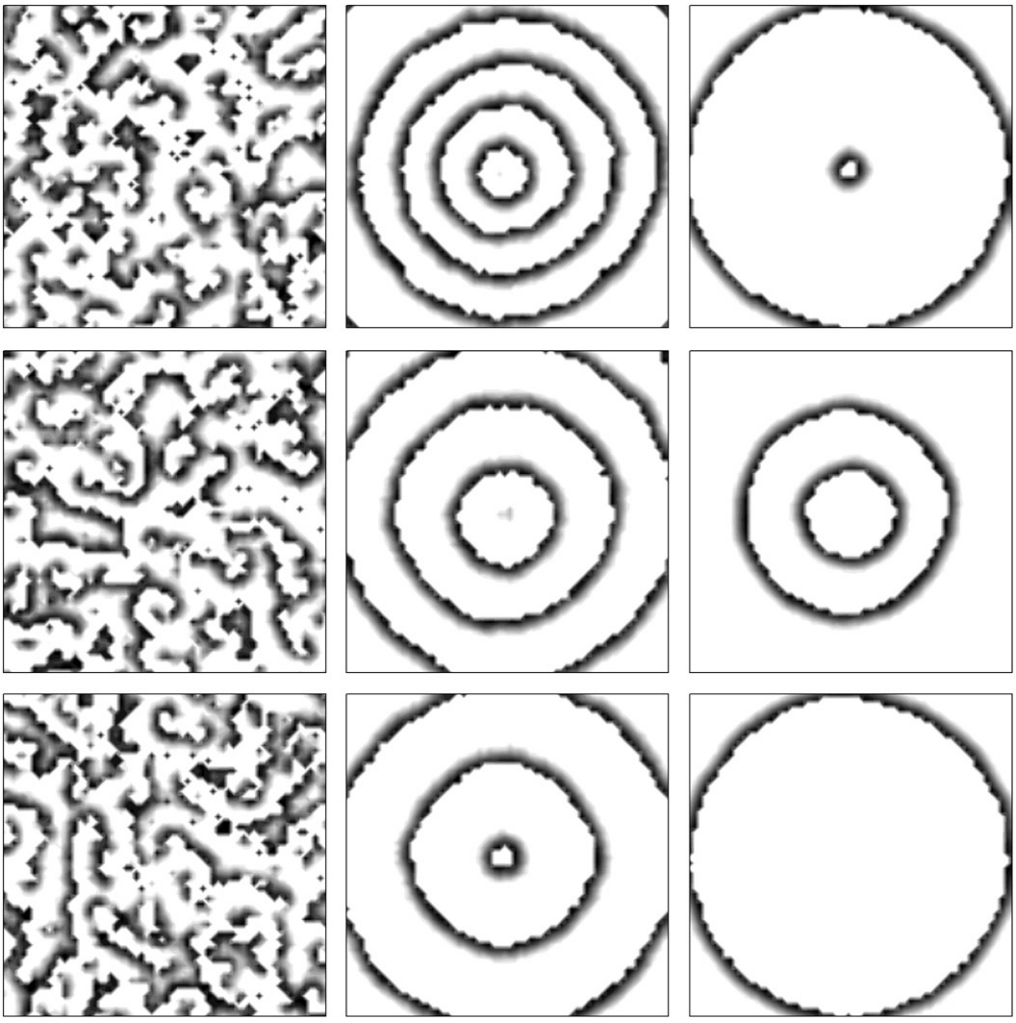

Fig. 2. Characteristic snapshots of the spatial profile of u for different χ and t_π. Columns vary in the employed system size of each excitable unit: $\chi = 50$ (left), $\chi = 200$ (middle), and $\chi = 800$ (right). Rows vary in the employed period of the pacemaker: $t_\pi = 0.8$ (top), $t_\pi = 1.2$ (middle), and $t_\pi = 1.6$ (bottom). All panels are drawn using a linear color profile white marking 0.0 and black 2π values of u.

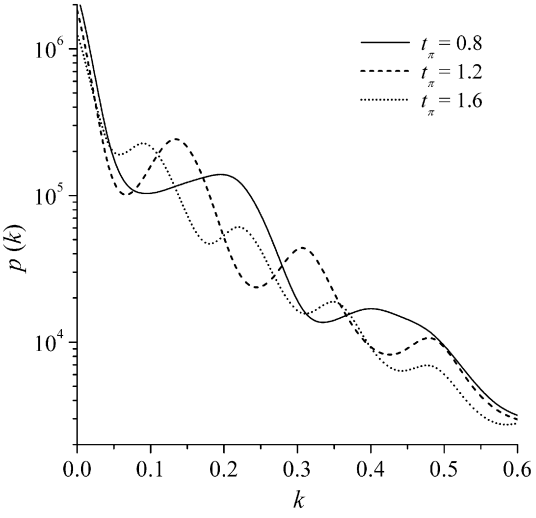

Fig. 3. Circularly averaged spatial structure functions of $u_{i,j}$ for different t_π obtained by the optimal level of internal noise $\chi = 200$.

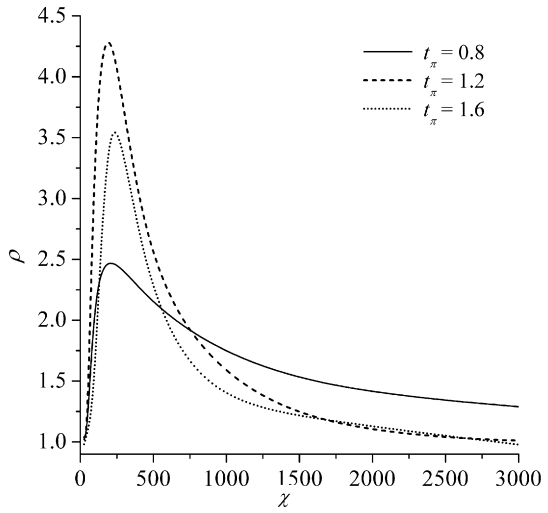

Fig. 4. Spatial order of excitatory waves ρ in dependence on χ for different t_π.

in Eq. (2) is small in comparison to the system size. Moreover, the pacemaker cells (those that are under the direct influence of the periodic pulse train) are rarely activated all at once, but often a single cell amongst the nine that is at the time most heavily perturbed by internal noise, is activated first. By using this simplified version of the model, we are able to analytically estimate

the relationship between the pacemaker activity and the patterns characterizing the spatial dynamics. Moreover, we are also able to identify necessary conditions for the pacemaker-guided noise-induced spatial periodicity in excitable media.

To reveal the relationship between the pacemaker activity and the spatial dynamics, we must link the oscillation period of the pacemaker t_π with the resonantly pronounced spatial frequency $k = k_{\max}$. Since $k_{\max} = 1/\lambda$, where λ is the wavelength representing the distance between two neighboring wave fronts, the relationship between t_π and $k_{\max}$ can obviously be determined easily, if one knows the expression for λ. The wavelength λ represents the distance travelled by the wave front between two pacemaker excitations. In other words, λ specifies exactly how many units of the spatial grid of size Δx are activated in one pacemaker period t_π, and can thus be expressed as

$$\lambda = \frac{t_\pi}{t_a}\Delta x, \tag{7}$$

where t_a is the so-called activation time. The activation time t_a is the time needed to transmit the signal from one unit to the other, i.e. the time needed to force a neighboring quiescent unit from its steady state at $u = 0$ to its threshold value $u = u_c$. In accordance with the treatment presented in [68], the excited unit has to overcome the internal resistance of the quiescent unit given by $\mathrm{d}u/\mathrm{d}t = 1-a$, which imposes a tendency towards $u = 0$. Thereby, the dynamics of the excited neighbour is determined by the fast kinetics $\mathrm{d}u/\mathrm{d}t = b$, and since $u_c \ll 2\pi$ the variable practically changes as $u = bt$. Hence, the dynamics of a quiescent unit, coupled with an already excited unit, can be described by the equation

$$\frac{\mathrm{d}u}{\mathrm{d}t} = 1 - a + D(bt - u). \tag{8}$$

Integrating Eq. (8) for the initial condition $u|_{t=0} = 0$ gives an implicit equation for t_a that reads

$$c\mathrm{e}^{-Dt_a} + bt_a = u_c + c, \tag{9}$$

where $c = (a + b - 1)/D$. In order to obtain an explicit expression for t_a we simplify Eq. (9) by applying the approximation $\mathrm{e}^{-Dt_a} \approx 1 - Dt_a + D^2t_a^2/2$. By retaining the physically relevant positive solution, and considering that $b \gg a - 1$, we obtain:

$$t_a \approx \frac{a - 1 + \sqrt{2bDu_c}}{bD}. \tag{10}$$

Importantly, when integrating Eq. (8), the initial state of variable u is actually [by numerical simulations of the spatially extended system given by Eq. (2)] not exactly zero, but in fact $u|_{t=0} = \varepsilon > 0$. We found that on average $\varepsilon = 0.35u_c$, which is a consequence of the internal stochasticity introduced in the above-studied spatially extended system. This has the same effect as if u_c in Eq. (10) is replaced by the effective threshold $0.65u_c$. By inserting Eq. (10) into Eq. (7) and calculating $k_{\max}(t_\pi) = 1/\lambda$, we obtain the analytically estimated dependence of $k_{\max}$ on t_π. In Fig. 5 we can see that the analytical estimation is in good agreement with the corresponding numerical simulations according to Eq. (2). Only for larger pacemaker oscillation periods, deviations of numerical computations become more considerable, since the numerical inaccuracy of the Fourier transformation increases by consequently larger spatial wavelengths, due to the finiteness of the spatial grid ($n = 64$).

Finally, it remains of interest to determine necessary conditions for the pacemaker-guided noise-induced spatial periodicity in excitable media presented in Section 3. To this purpose, we point out the importance of the minimal refractory time $t_{\min} = \min\{t_r\}$, which is required for an efficient external forcing, specifically by preventing an undesired spreading of excitatory events. More

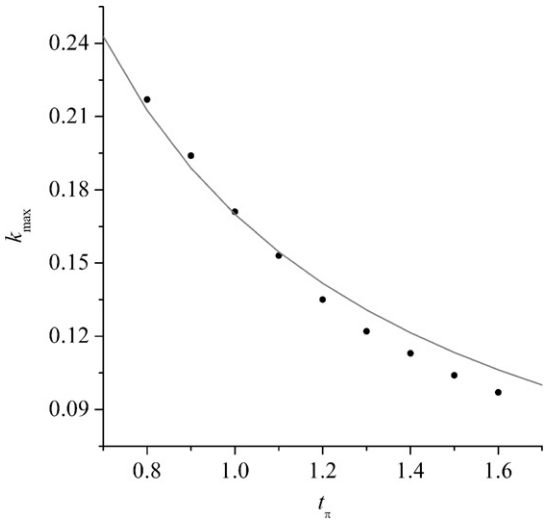

Fig. 5. Dependence of spatial wave number $k_{\max}$ on the pacemaker oscillation period. Symbols indicate numerically obtained values, whilst the grey solid line indicates the analytically estimated dependence.

precisely, $t_{\min}$ has to be large enough to prevent a feedback effect and, with it, related undesired (premature) reactivation of those units that lie in the opposite direction of the spreading direction of the excitatory wave. Particularly problematic is the situation in the pacemaker unit. Note that in all other units the phase difference between neighboring units is t_a, and hence $t_{\min} \approx t_a$. However, for the pacemaker unit this is only true if the sub-threshold pacemaker signal, together with noise, just reaches the threshold (evokes an excitation). This is actually the case in our model. However, in a more general setting the pacemaker signal may exceed the threshold (suprathreshold pacemaker). Then $t_{\min} > t_a$ and must be defined as follows:

$$t_{\min} = (t_a + t_e) - (t_f + t_p), \tag{11}$$

where t_e is the excursion time of non-pacemaker units and equals the width of the spikes. The excursion time can be estimated as $t_e \approx 2\pi/b$, because $b >> a - 1$ and $u_c << 2\pi$. The times t_f and t_p relate to the pacemaker. Specifically, t_f is signal duration in the pacemaker unit when $\pi_\Theta = g$ [see Eq. (3)] and $u > u_c$, while t_p is the duration of the spike in the pacemaker unit when $\pi_\Theta = 0$ and $u > u_c$. Since a lot of time scales are used, in Table 2 we provide a list with short descriptions of all time scales used in the calculations, in order to clarify the issue in this section. The calculation of $t_{\min}$ requires the determination t_p. It can be estimated by considering the dynamics of the pacemaker unit when $\pi_\Theta = 0$. Since $u > u_c$, the dynamics in the pacemaker unit are determined by the fast kinetics $\mathrm{d}u/\mathrm{d}t = b$; however, reduced for the leak $\mathrm{d}u/\mathrm{d}t = -D(u - bt)$ into four neighbouring cells. Hence we have:

$$\frac{\mathrm{d}u}{\mathrm{d}t} = b - 4D(u - bt). \tag{12}$$

Eq. (12) is mathematically equivalent to Eq. (8) and can be solved in an analogous way. The only difference is that Eq. (12) has to be integrated for the initial condition $u|_{t=0} = u_0$, where $\mathrm{d}u_0/\mathrm{d}t = g$ and $u_0 \approx gt_f$. The integration of Eq. (12) gives the following implicit expression for t_p:

$$u_0\mathrm{e}^{-4Dt_p} + bt_p = 2\pi. \tag{13}$$

In order to obtain an explicit expression we simplify Eq. (13) by applying the approximation $\mathrm{e}^{-4Dt_{PM}} \approx 1 - 4Dt_p + \frac{1}{2}(4D)^2t_p^2$. By retaining the physically relevant positive solution, and considering that $b \gg a - 1$, we obtain:

$$t_p \approx \frac{4Du_0 - b + \sqrt{(b - 4Du_0)^2 - 32u_0D^2(u_0 - 2\pi)}}{16u_0D^2}. \tag{14}$$

Table 2
A list of time scales employed in the analytical estimation.

Symbol	Description
t_π	Pacemaker oscillation period
w	Pacemaker pulse duration
t_a	Activation time of a non-pacemaker unit
t_e	Excursion time of a non-pacemaker unit
t_f	Signal duration in the pacemaker unit when $\pi_\Theta = g$ and $u > u_c$
t_p	Signal duration in the pacemaker unit when $\pi_\Theta = 0$ and $u > u_c$
t_r	Refractory time – the time that sets in after each excitation and provides $u \equiv 0$
$t_{\min}$	Minimal refractory time: $t_{\min} = \min\{t_r\}$

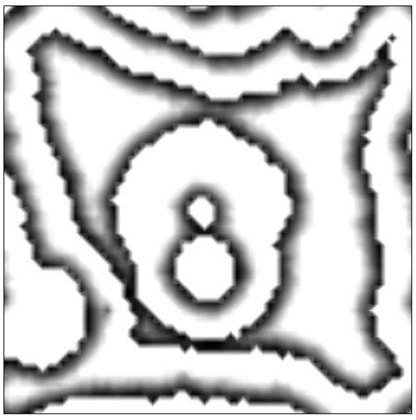

Fig. 6. Characteristic snapshot of the spatial profile of u obtained for $\chi = 200$ (optimal level of internal noise), $t_\pi = 1.2$, and $t_r = 0.16$. Clearly, if the refractory time is too small, the pacemaker loses the ability to guide the spatial dynamics and the inherent spatial frequency predominates the dynamics. The color-coding is the same as in Fig. 2.

By inserting Eq. (14) into Eq. (11) we get the analytical approximation for the minimal refractory time $t_{\min}$.

As already mentioned above, in the special case when the subthreshold pacemaker signal together with noise just barely reaches the threshold ($t_f \approx 0$ and $t_p \approx t_e$), as it is the case in our model, the estimation for the minimal refractory time simplifies to $t_{\min} \approx t_a$. To demonstrate that the condition $t_r > t_{\min}$ is indeed a necessary one for an efficient pacemaker-guided noise-induced spatial periodicity in the studied medium, Fig. 6 features a simulation when $t_r = 0.16 < t_{\min} \approx t_a = 0.17$ [the latter value was calculated according to Eq. (10) with the system parameters used in Section 3]. Evidently, the circular waves are disrupted, because a too short refractory time leads to unwanted spreading of excitatory events. Therefore, the wavelength of excitatory waves guided by the pacemaker is completely overshadowed by the system's intrinsic spatial wavelength, which depends on t_r [69]. So, an efficient pacemaker regulation (guidance) of the spatial dynamics clearly requires that $t_r > t_{\min}$.

The existence of a finite $t_{\min}$ is also related to the decrease of the maximally attainable ρ by $t_\pi = 0.8$, reported in Fig. 4. Namely, the necessity for a non-zero refractory time $t_{\min}$ imposes a lower bound for the period of the pacemaker because several events must happen inside t_π [activation via the pulse (t_a), excitation (t_e), and finally the refractory time (t_r)] in order for the pacemaker to be effective. If determined analytically, the duration of all these events ($t_a + t_e + t_r \approx 0.75$ for parameters used in Section 3) is smaller than $t_\pi = 0.8$. However, since we are dealing with an inherently stochastic system, which we have not explicitly considered by our above analytical estimations, disruptive effects lowering ρ set in already by t_π that are somewhat larger than the minimally required value ($t_a + t_e + t_r$). Specifically, these effects are related to noise-induced modifications of critical times (t_a and t_e), which if operating close to the boundary values of t_π, may result in pacemaker activity during t_r and with it related failure to trigger a wave, finally reflecting in lower values of ρ as shown in Fig. 4. Of course, these stochasticity-related effects become less pronounced as t_π increases since the error margins for t_a and t_e, still warranting effective pacemaker guidance of excitatory events, increase as well. In conclusion, results presented in Fig. 4 and 6 succinctly demonstrate the importance of an appropriate length of the refractory time (and with it the related period of the pacemaker), which turns out to be a necessary, but also sufficient condition for pacemaker-guided spatial periodicity in excitable media.

5. Pacemaker-guided noise-induced Ca^{2+} waves

While the system given by Eq. (1) incorporates only the minimal dynamical ingredients warranting excitable behavior, it nonetheless has features that are inherent in a wide array of physiological scenarios. Among the most prominent examples of excitable systems with fast dynamics during the spike and slow dynamics during the quiescence phase, are those of the membrane potential in neural and cardiac cells, where the formalism developed by Hodgkin and Huxley [70] still forms the core of most currently employed mathematical models. More specifically, ionic mechanisms warranting excitability in neural tissue rely on the increase in the membrane potential and opening of Na^+ or Cl^- channels, and with it related rapid influx of the ions, as well as on the subsequent comparatively slow process of closing the channels and activation of K^+ channels. Although the exact modelling, taking into account specific physiological processes, usually leads to a fairly complex set of differential equations [66,70], the dynamics of the two main fast and slow processes can be qualitatively captured by Eq. (1).

Moreover, oscillations of free cytosolic calcium concentration in excitable and non-excitable cells, which play a crucial role in regulating several cellular processes, are another example of the combined effects of fast and slow dynamics [62,63]. Usually, Ca^{2+} spikes are separated by quiescent phases, because after the fast calcium release from the endo/sarco plasmic reticulum (ER/SR) much slower processes of calcium binding to cytosolic proteins, its sequestration in mitochondria, and finally pumping back into the ER/SR take place [63]. However, as by the modelling of neural and cardiac dynamics, the complexity of mathematical models for Ca^{2+} oscillations resulting from taking into account specific physiological processes [62,63] can be, at least in terms of some dynamical features, reduced to that of Eq. (1). Thus, Eq. (1) models excitability as a canonical dynamical property [66] of physiologically accurate models without taking explicitly into account specific underlying physiological details of such processes.

Here we study the impact of internal noise and a subthreshold pacemaker on the spatial dynamics of diffusively coupled cells in which the local dynamics is determined by the theoretical framework of Somogyi and Stucki [71], which represents a mathematical model describing inter-cellular Ca^{2+} dynamics. Specifically, the model considers changes of free Ca^{2+} concentration in the cytosol (Ca_{cyt}) and in the intracellular calcium store (Ca_{ER}). Individual cells are arranged on a $L \times L$ ($i, j \in [1, L]$) square lattice and are diffusively coupled through the cytosol, which is modelled by an additional flux of the form $D\nabla^2 Ca_{cyt}^{i,j}$. So, the spatial extension of the model has the following form:

$$\frac{dCa_{cyt}^{i,j}}{dt} = k_1 Ca_{ER}^{i,j} - k_2 Ca_{cyt}^{i,j} + \alpha Ca_{ER}^{i,j} \frac{(Ca_{cyt}^{i,j})^4}{K_s^4 + (Ca_{cyt}^{i,j})^4} + \gamma - \beta Ca_{cyt}^{i,j} + D\nabla^2 Ca_{cyt}^{i,j} + \pi_\Theta(t), \quad (15)$$

$$\frac{dCa_{ER}^{i,j}}{dt} = k_2 Ca_{cyt}^{i,j} - k_1 Ca_{ER}^{i,j} - \alpha Ca_{ER}^{i,j} \frac{(Ca_{cyt}^{i,j})^4}{K_s^4 + (Ca_{cyt}^{i,j})^4}, \quad (16)$$

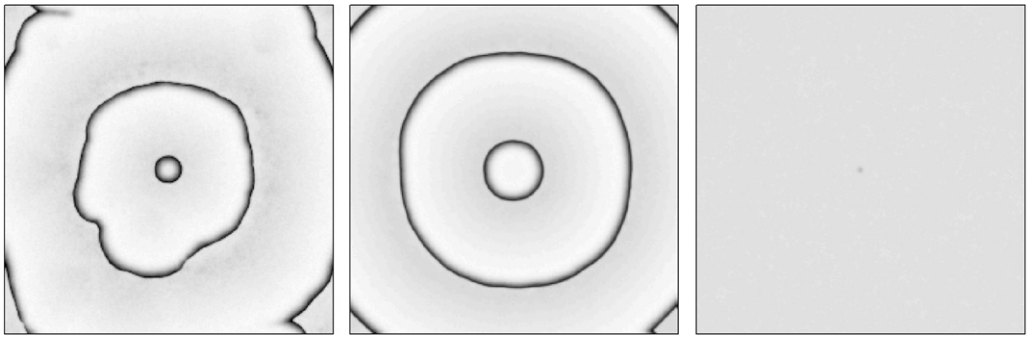

Fig. 7. Characteristic snapshots of the spatial profile of $Ca_{cyt}^{i,j}$ for different cell volumes: $V = 1.0$ (left panel), $V = 5.0$ (middle panel), $V = 7.0$ (right panel). All snapshots are depicted on square grids with linear size $L = 256$ and a linear color profile, where white depicts 0.5 and black 4.5 values of $Ca_{cyt}^{i,j}$. The employed system parameters are: $k_1 = 0.1, k_2 = 1.0, \alpha = 18.0, \beta = 1.0, \gamma = 1.0, K_S = 3.5, D = 1.1, t_\pi = 23.0, w = 5.0, g = 0.21$.

Table 3
Reaction rates and corresponding stochastic processes entailed in a given iteration of the employed τ-leap algorithm for the Somogyi & Stucki model [71].

Reaction rate:	Stochastic process:
$r_1 = N_A V k_1 Ca_{ER}^{i,j}$	$Ca_{cyt}^{i,j} \to Ca_{cyt}^{i,j} + \kappa_1/N_A V,\ Ca_{ER}^{i,j} \to Ca_{ER}^{i,j} - \kappa_1/N_A V$
$r_2 = N_A V k_2 Ca_{cyt}^{i,j}$	$Ca_{cyt}^{i,j} \to Ca_{cyt}^{i,j} - \kappa_2/N_A V,\ Ca_{ER}^{i,j} \to Ca_{ER}^{i,j} + \kappa_2/N_A V$
$r_3 = N_A V \alpha Ca_{ER}^{i,j} \frac{(Ca_{cyt}^{i,j})^4}{K_s^4 + (Ca_{cyt}^{i,j})^4}$	$Ca_{cyt}^{i,j} \to Ca_{cyt}^{i,j} + \kappa_3/N_A V,\ Ca_{ER}^{i,j} \to Ca_{ER}^{i,j} - \kappa_3/N_A V$
$r_4 = N_A V \gamma$	$Ca_{cyt}^{i,j} \to Ca_{cyt}^{i,j} + \kappa_4/N_A V$
$r_5 = N_A V \beta Ca_{cyt}^{i,j}$	$Ca_{cyt}^{i,j} \to Ca_{cyt}^{i,j} - \kappa_5/N_A V$
$r_6 = N_A V D \left\lvert Ca_{cyt}^{i+1,j} - Ca_{cyt}^{i,j} \right\rvert$	$Ca_{cyt}^{i,j} \to Ca_{cyt}^{i,j} + \kappa_6/N_A V,\ Ca_{cyt}^{i+1,j} \to Ca_{cyt}^{i+1,j} - \kappa_6/N_A V$ for $Ca_{cyt}^{i+1,j} - Ca_{cyt}^{i,j} > 0$ $Ca_{cyt}^{i,j} \to Ca_{cyt}^{i,j} - \kappa_6/N_A V,\ Ca_{cyt}^{i+1,j} \to Ca_{cyt}^{i+1,j} + \kappa_6/N_A V$ for $Ca_{cyt}^{i+1,j} - Ca_{cyt}^{i,j} < 0$
$r_7 = N_A V D \left\lvert Ca_{cyt}^{i-1,j} - Ca_{cyt}^{i,j} \right\rvert$	$Ca_{cyt}^{i,j} \to Ca_{cyt}^{i,j} + \kappa_7/N_A V,\ Ca_{cyt}^{i-1,j} \to Ca_{cyt}^{i-1,j} - \kappa_7/N_A V$ for $Ca_{cyt}^{i-1,j} - Ca_{cyt}^{i,j} > 0$ $Ca_{cyt}^{i,j} \to Ca_{cyt}^{i,j} - \kappa_7/N_A V,\ Ca_{cyt}^{i-1,j} \to Ca_{cyt}^{i-1,j} + \kappa_7/N_A V$ for $Ca_{cyt}^{i-1,j} - Ca_{cyt}^{i,j} < 0$
$r_8 = N_A V D \left\lvert Ca_{cyt}^{i,j+1} - Ca_{cyt}^{i,j} \right\rvert$	$Ca_{cyt}^{i,j} \to Ca_{cyt}^{i,j} + \kappa_8/N_A V,\ Ca_{cyt}^{i,j+1} \to Ca_{cyt}^{i,j+1} - \kappa_8/N_A V$ for $Ca_{cyt}^{i,j+1} - Ca_{cyt}^{i,j} > 0$ $Ca_{cyt}^{i,j} \to Ca_{cyt}^{i,j} - \kappa_8/N_A V,\ Ca_{cyt}^{i,j+1} \to Ca_{cyt}^{i,j+1} + \kappa_8/N_A V$ for $Ca_{cyt}^{i,j+1} - Ca_{cyt}^{i,j} < 0$
$r_9 = N_A V D \left\lvert Ca_{cyt}^{i,j-1} - Ca_{cyt}^{i,j} \right\rvert$	$Ca_{cyt}^{i,j} \to Ca_{cyt}^{i,j} + \kappa_9/N_A V,\ Ca_{cyt}^{i,j-1} \to Ca_{cyt}^{i,j-1} - \kappa_9/N_A V$ for $Ca_{cyt}^{i,j-1} - Ca_{cyt}^{i,j} > 0$ $Ca_{cyt}^{i,j} \to Ca_{cyt}^{i,j} - \kappa_9/N_A V,\ Ca_{cyt}^{i,j-1} \to Ca_{cyt}^{i,j-1} + \kappa_9/N_A V$ for $Ca_{cyt}^{i,j-1} - Ca_{cyt}^{i,j} < 0$
$r_{10} = N_A V \pi_\Theta$	$Ca_{cyt}^{i,j} \to Ca_{cyt}^{i,j} + \kappa_{10}/N_A V$

where α, β, γ, k_1, k_2 and K_s are constants as originally used by Somogyi and Stucki [71]. The subthreshold pacemaker $\pi_\Theta(t)$ has the same form as defined in Eq. (3) and is also active only in the central 9 units of the medium. The employed system parameters are quoted in the caption of Fig. 7. The excitability of the cells is initiated by placing the cells into a steady state just before the Hopf bifurcation occurring at $\alpha \approx 19.2$ in the deterministic model. So, without taking into account the internal stochasticity due to finite sizes of cellular compartments and related small numbers of reacting ions participating in the dynamics, the subthreshold pacemaker would not be capable of activating the cells and the medium would remain quiescent.

Analogous to the canonical model presented in Section 2, we integrate the resulting spatial extended system (15) and (16) via Gillespie's τ-leap method. We emphasize once more that, as exemplified by Gracheva et al. [59] and Li et al. [10], reaction rates are ascribed to fluxes that are concerned in the model. In this manner all the processes in the cell can be grouped into ten elementary processes, which correspond to prescribed reaction rates and are given in Table 3. In accordance with those reaction rates, a discrete change of the Ca^{2+} concentration of the form $\kappa_x/N_A V$ is performed at each iteration (as defined in Table 3), where N_A is Avogadro's number, V is the volume of each individual cell and κ_x is an integer obtained from Eq. (4).

In Fig. 7 we show characteristic snapshots of the spatial profile of the coupled cells for three different systems sizes. It can be seen that the subthreshold pacemaker activity induces most coherent calcium waves at an intermediate value of V. For small volumes, the internal noise disturbs the wave coherence. On the other hand, if the system size is too large, the intensity of fluctuations is too low to provoke excitations of the cells and the ensemble of coupled cells remains quiescent. Only an intermediately pronounced level of stochasticity is able to optimally support the pacemaker activity and thus warrant the most clear and expressive spatial frequency.

In order to further elaborate on this visual assessment we calculate the spatial structure function (Eq. (5)), only that here $H(k_x, k_y, t)$ represents the spatial Fourier transform of the $Ca_{cyt}^{i,j}$ field. By continuing with the same procedure as described in Section 3, we calculate the quantity ρ for different volumes. Fig. 8 shows how ρ varies with the employed system size. It is evident that there exists an optimal intensity of internal noise, for which the peak of the circularly averaged structure function is, at best, pronounced. The clear maximum at $V \approx 5$ thereby indicates the optimal system size for the greatest coherence of calcium waves triggered by the subthreshold pacemaker.

By comparing Fig. 8 with Fig. 4, and also Fig. 7 with Fig. 2, we see that the results for the simple analytically tractable model (Eq. (1)) and those for a more complex biologically relevant model are qualitatively the same. In both cases, the results clearly indicate the importance of the refractory time, enabling a well-controllable regulation of spatial dynamics by a subthreshold pacemaker in presence of noise. While the refractory time in biological systems occurs naturally, it is adjustably introduced in the more simple